11th ANKARA INTERNATIONAL AEROSPACE CONFERENCE **AIAC-2021-014**
8-10 September 2021 - METU, Ankara TURKEY

ADJOINT BASED AERODYNAMIC SHAPE OPTIMIZATION OF A FLUSH INLET WITH SU2

Ali Ahmed* and Ismail H. Tuncer†
Middle East Technical University
Ankara, Turkey

ABSTRACT

In this study the aerodynamic shape optimization of a subsonic flush inlet is performed. The total pressure at the AIP and lift are employed as a combined objective function and the drag is constrained. Open-ware platforms are used including SALOME for solid modeling, GMSH for the hybrid mesh generation and SU2 for flow solutions and adjoint based shape optimization. Multiple free form deformation FFD boxes enclose different regions of the inlet for shape parameterization and surface deformation. A flush inlet geometry from reference study is taken as the baseline configuration. The inlet surface is then allowed to deform along the optimization steps. The optimum shape produces a deformation at the inlet duct surface. The total pressure recovery at AIP is improved by 3% and an additional C_L/C_D ratio of 0.011 for the overall vehicle is achieved. The drag is constrained and remains within nominal range from the baseline value.

INTRODUCTION

Flush type or fully submerged inlet was a major candidate viz-a-viz pitot inlet during the early days of the jet age. However due to issues such as comparatively lower pressure recovery at transonic conditions the pitot type was given preference and flush inlet more or less was ignored [Mossman, 1947]. On the other hand flush inlet are inherently devoid of form drag and have lower RCS signature therefore in many applications flush inlet are considered due to these advantages. Consequently, these type of inlets found their place in auxiliary applications for cabin pressure and cooling air but not in propulsion systems.

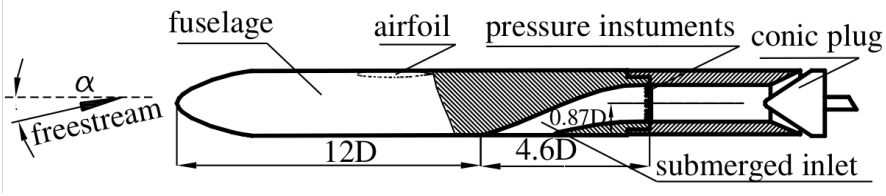

Figure 1: Flush inlet configuration by Shu Sun et al [Sun Shu, 2007]

*PhD Graduate in Aerospace Engineering Department, Email: ali.ahmed_01@metu.edu.tr
†Prof. Dr. and Chairman Aerospace Engineering Department, Email: ismail.h.tuncer@ae.metu.edu.tr

Preliminary studies of flush inlet for air breathing engines in slender bodies were conducted due to the obvious benefits due to RCS. Lee studied the consequence of varying inlet geometric parameters on the performance such as pressure recovery at Aerodynamic Interface Plane (AIP) by using commercial CFD code [Lee, 2004]. Sun and Guo [Sun, 2005] studied the performance for flush mounted planar side inlet . Later in a inlet performance characterization study, Sun [Sun Shu, 2007] optimized three geometric parameters side edge angle, ramp angle and curvature of rear lip . This study encompassed both experimental and numerical results. The top face projection of the flush inlet is trapezoidal when placed in a slender body which makes it non-generic with respect to the well established NACA type flush inlet. The inlet performance was found to be maximum at a ramp angle of 23° and side edge single of 4° as shown in figure 1. Distortion coefficient DC was also found to be minimum at the same values of the given angles.

Most of the shape optimization studies carried out on subsonic inlet with bend duct were carried out with an intention of minimizing the distortion at the AIP or maximizing total pressure recovery however both parameters are complimentary and improvement in one almost usually benefits the other. This is due to the flow behavior which defines distortion. Distortion is a measure of secondary flow relative to the primary flow and therefore if the primary flow is getting a swirl while reaching the AIP in the inlet duct it usually subdues the secondary flows. This phenomenon was utilized by Taskinoglu [Taskinoglu, 2004]. A swirl device in the form of VG fin was placed inside the s-duct of the inlet and the variables of the study were its geometrical parameters i.e. fin height, length and incidence angle while objective functions were distortion and swirl indices over the AIP. Genetic Algorithm (GA) was employed as optimized using trade-off or ϵ-constraint method for finding the Pareto optimal set . The principal benefit of the fin is the generation of a large tip vortex within the inlet, which substantially modifies the flowfield. The distortion index using two inlet configurations was observed to be reduced by 25% and 70% respectively at the expense of a substantial increase in swirl index in both however the pressure recovery only slightly improved. Joon also employed VG inside a inlet duct to enhance performance and inventively employed adjoint based shape optimization [Joon, 2012].

Cheng placed bleed slots and optimized the performance for the flush inlet in a slender body. By varying the bleed flow rate the total pressure recovery increased by 2.8% and DC decreased by 51.0% [Cheng, 2012]. Later, Sun, Tan and Wang used a unique bump placed on the body upstream of the inlet to increase the total pressure recovery of the submerged inlet by 3.7% however drag penalty increased by a max of 0.76% which was calculated for the complete slender body including the inlet [Tan, 2016].

It is evident from the aforementioned studies that most of the efforts to improve the performance of flush inlet was undertaken by adding devices such as VG or bleeding air and less emphasis was on the actual shape of the inlet. The present study takes the opportunity to optimize the shape of the inlet based on the available performance parameters as well as investigate additional parameters such as lift which may add to the capabilities of such inlets while employing adjoint based optimization techniques.

METHOD

The methodology of aerodynamic shape optimization as followed in the study is illustrated in figure 2. The general sequence is based upon solid modeling , mesh generation , CFD flow and adjoint solver and shape deformation. The reference trapezoidal intake geometry and placement in the slender body as show earlier is modeled in SALOME with 4° side edge angle and 23° ramp angle and location is at the same ratios while some arbitrary dimensions are used since exact geometric specifications such as AIP diameter and duct curvature splines are not available. The modeled geometry is flipped over such that the intake faces towards the positive y-direction as shown in figure 3. This is done in order to align the geometry for lift optimization.

The size of the computational domain is a 3D rectangular farfield which is 20 times the body

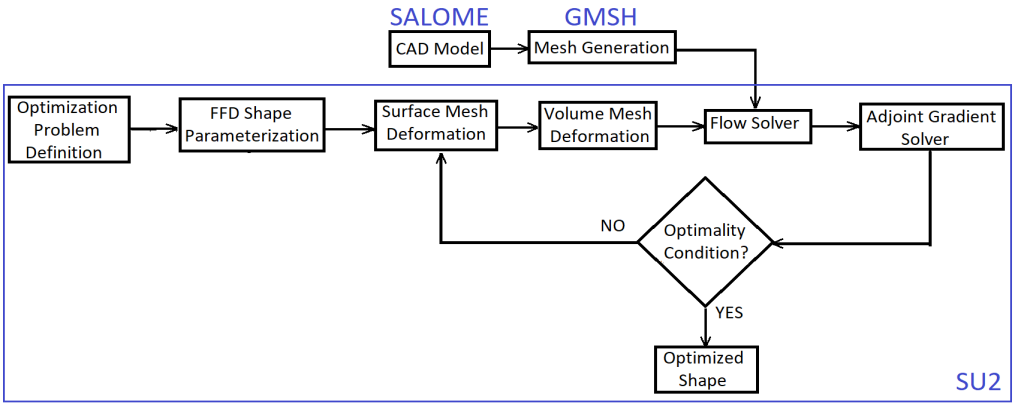

Figure 2: Design cycle process.

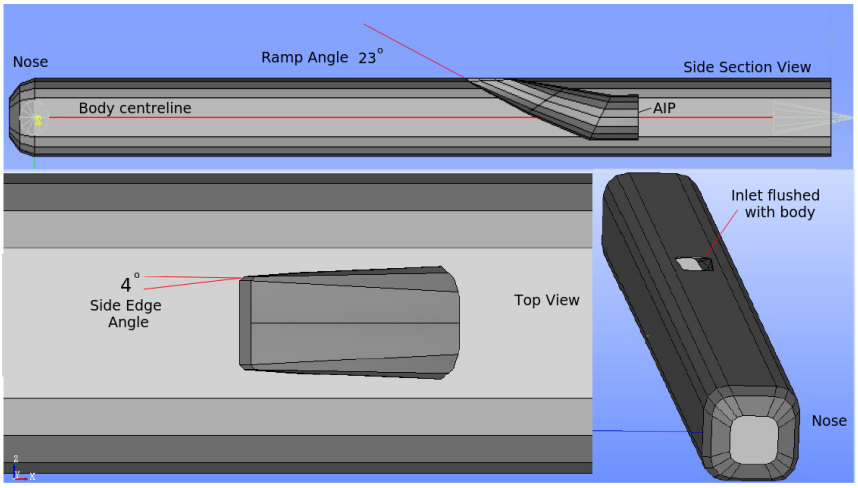

Figure 3: Solid modeling with SALOME.

diameter in the side direction and 20 times the length of the body in axial direction with the body at center. GMSH is used to generate hybrid 3D mesh with a boundary layer zone as shown in figure 4. GMSH is a open source tool which generates the desired .su2 mesh. The extrude feature in GMSH is employed for prism layering with gradual size steps to resolve viscous boundary layer over which the unstructured tetrahedral cells for outer mesh is created. The height of the wall adjacent cell is 1.6e-06 m which is calculated for Mach number = 0.7 and Reynolds no = 1.56e6. Note that the last prism layer cell before the unstructured mesh starts is almost square cross section. The direct solution for the case is run in SU2 direct flow solver for for Mach number = 0.7 and Reynolds number = 1.56e6 for mesh sensitivity study. Wall surfaces taken at adiabatic condition (Heat flux = 0). The intake AIP is taken at $p_2/P_0 = 0.8$ as the outlet boundary condition. The turbulent flow solutions are obtained on a baseline mesh as well as the solution adapted mesh. SST model are used to resolve the flow. The Y+ distribution on surface due to flow solution is shown in figure 5. The Y+ is less than 1 for most of the surfaces however around the edges Y+ distribution is found to increase to value of 4. Mesh independence is achieved through the mesh adaptation process. The baseline mesh is adapted repeatedly by employing flow gradient based adaptation whereby the number of cells is allowed to increase by twice. The mesh size and solution obtained at each adaptation level in terms of total pressure recovery factor is given in table 1. As seen, the resultant mesh after the first adaptation step with 1.55 million cells provides a converged solution and differs from the reference study by -0.504%. Therefore it is taken as the optimum mesh

which provides mesh independent solutions and is used for the verification and optimization studies. Larger number of cells obtained only increase the computational cost without considerable accuracy gains. SU2 solves Reynolds averaged Navier-Stokes RANS equations and corresponding values of the objective function. As shown in the flow chart in figure 2 the baseline geometry and solution is thereafter optimized using design cycles in which deformation, adjoint calculation and direct solver is used iteratively till optimized design is achieved.

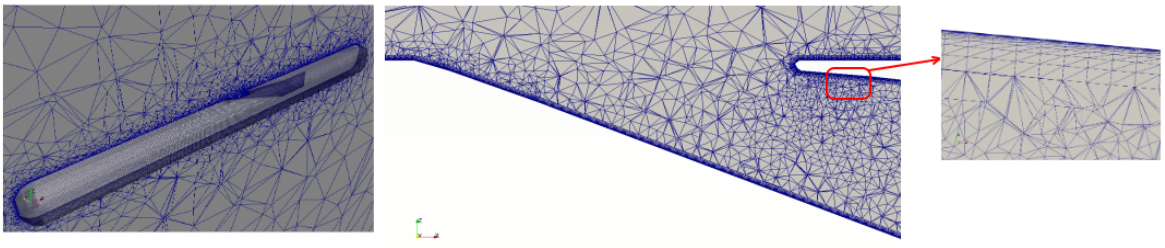

Figure 4: Hybrid mesh generation with GMSH.

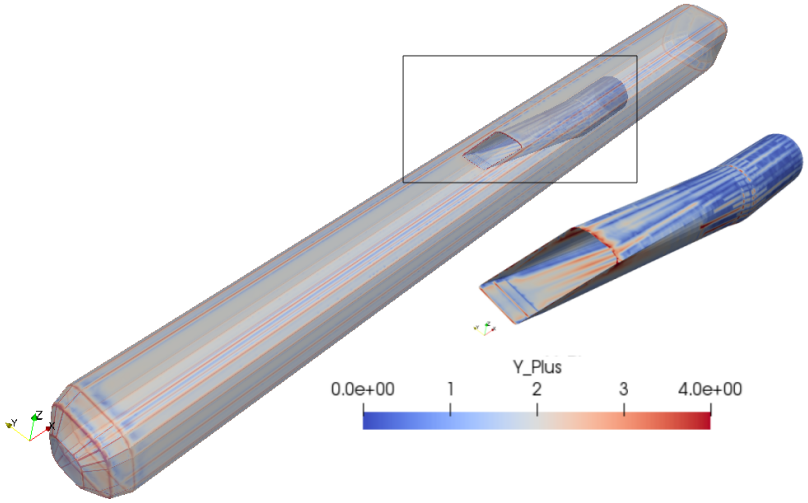

Figure 5: Y+ distribution on slender body and intake wall surfaces.

Table 1: Mesh Independence study at $M = 0.7$ and $\alpha = 4^\circ$.

Mesh Size	Pressure Recovery	Difference%
750,000	0.8935	1.380
1,550,000	0.898	-0.504
2,500,000	0.899	-0.111
3,250,000	0.8995	-0.056
6,020,000	0.8996	-0.011
[Sun Shu, 2007]	0.906	-

Solutions are performed on the parallel computer system which is in the HPC lab of METU Center for Wind Energy (RÜZGEM). The cluster consists of 8 nodes with 4 AMD® Opteron™ 6276 CPUs (16 cores, clocked at 2.30 GHz) per node, totaling up to 512 cores. The convergence time of each CFD solution and adjoint is 2 hours each approximately while an additional 2-2.5 hours are required for each design for mesh deformation depending upon the degree of deformation . Therefore for a 100 design cycle optimization 280 hours are approximately required.

RESULTS AND DISCUSSION

Aerodynamic shape optimization of subsonic submerged inlet is performed using adjoint based method in SU2 suite. Flow solution is obtained for the baseline and results are compared with reference study. Thereafter adjoint based aerodynamic shape optimization of the flush submerged inlet is performed.

Flow solution and validation

The flow solved on the baseline is compared for total pressure recovery at the AIP in the previous section which suggests good agreement of results.

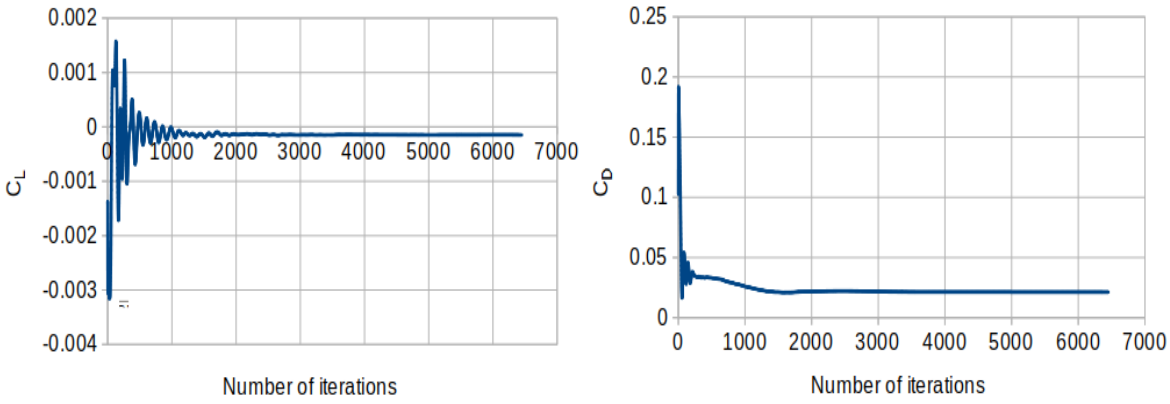

Figure 6: Convergence history for trapezoidal intake on slender body at Mach number 0.7.

The convergence history for the baseline case is shown in figure for lift and drag coefficients achieving constant values at around 1500 iterations. The pressure recovery factor is at 0.88 for the baseline which is is within 2 percent of the reference study as shown in figure 7 at $M = 0.7$ and $\alpha =$ 4deg.

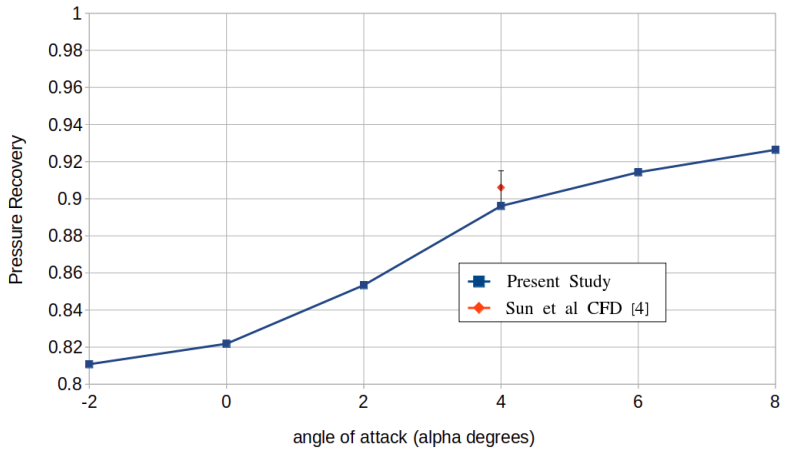

Figure 7: Pressure at AIP at different angle of attack.

Both qualitative and quantitative verification of the flow solutions are carried out for the baseline configuration. The Mach number contours are presented and favorably compared to the reference study in figure 6. It is observed that flow enters the inlet smoothly and remains attached along the ramp however on the the lip side of duct

Flow solution as Mach coloured streamlines are shown in figure 9. surface flow separates aft of the lip. The separation is accompanied by a local shock formation at the lip. The flow separation causes pressure losses but at the same time helps the pressure over the duct upper surface decrease and thus creates the pressure differential in favour of generating a lifting force. For a clean body with

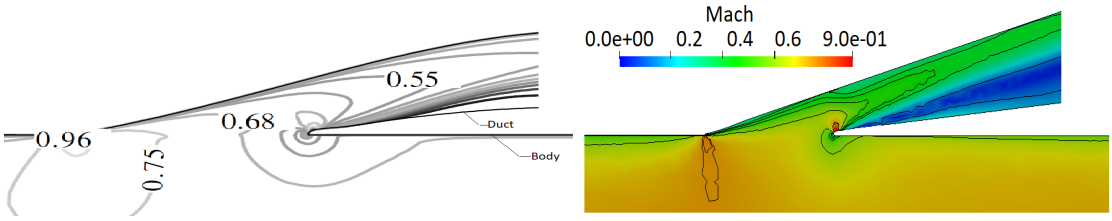

Figure 8: Mach contours. left: Reference study [Sun Shu, 2007] Right: Baseline solution.

no inlet cavity, the net force lateral to body is zero at zero angle of attack, in other words lift does not exist for such a symmetric flow but in the present study the flow enters the flush inlet laterally in an asymmetric fashion and contributes to the lift generation.

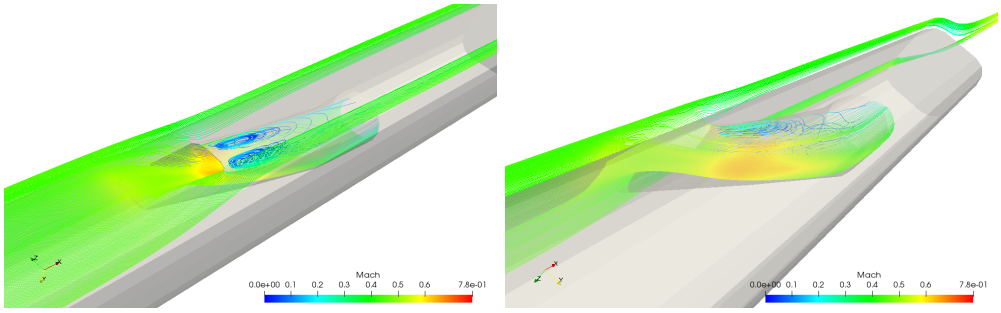

Figure 9: Mach colored streamline around intake.

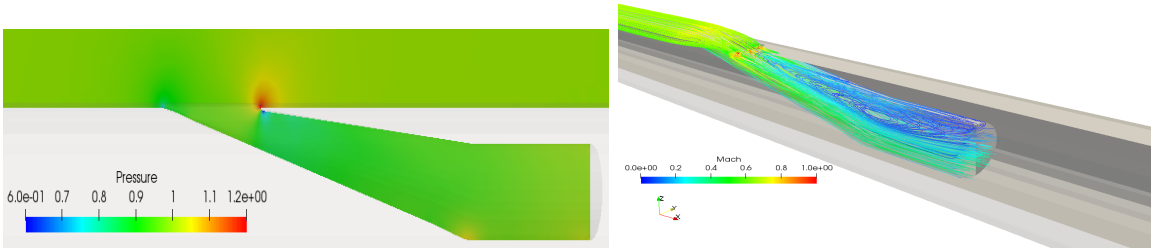

Figure 10: Baseline results: Pressure distribution (left); Mach colored streamline (right).

Shape optimization study

The shape optimization of the intake requires specification of the design variable surfaces. In this study, the intake remains flush with the body such that body surfaces remain intact as shown in figure 11. The design surfaces include the intake duct only which deform accordingly during optimization and improvement in performance relate to the shape variation in the internal flow through duct.

Multiple FFD boxes approach is undertaken for this case. There are two FFD boxes placed over the design space as shown in figure 12. The ramp surface leading from the fore lip to the AIP pipe is enclosed by red FFD box while the rear lip and portion of duct downstream is enclosed by blue FFD box. Both FFD boxes of (8,6,6) configuration provide a total of 2x441 control points. The main feature of this case is the simultaneous deformation process of multiple FFD boxes operating over a design surface.

The adjoint sensitivity distribution of the combined objective for baseline and optimum design are compared in figure 13. The regions in and around the inlet cavity are visibly prominent. It should be noted that at the end of the optimization process the surface sensitivities reduce to give almost negligible distribution at the optimum design.

The optimization history for the objective function as total pressure at AIP is given in figure 14.

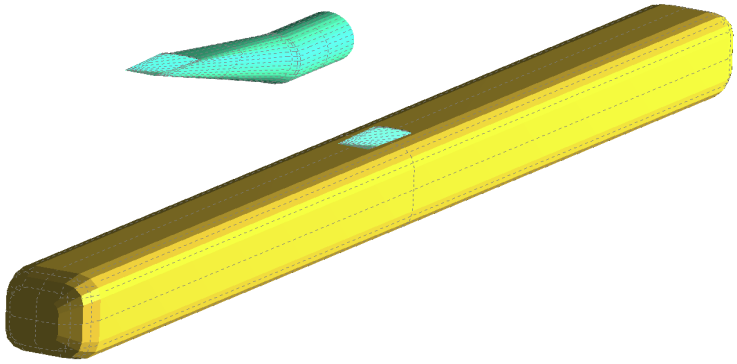

Figure 11: Design variable surfaces in blue with and without full body in yellow.

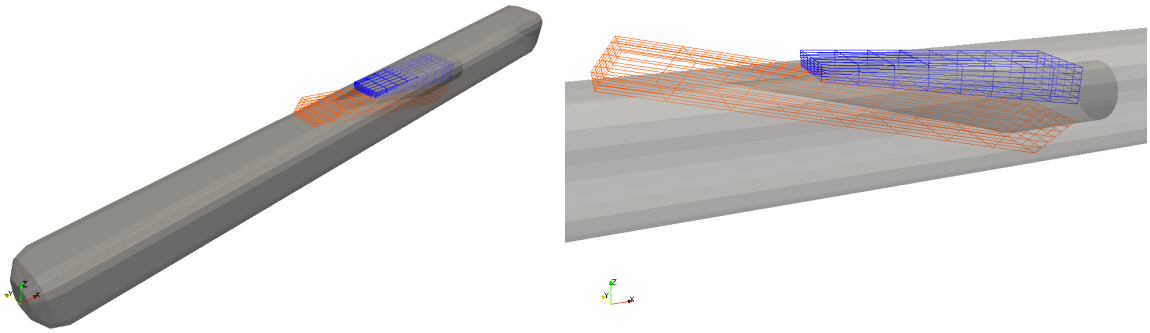

Figure 12: Multiple FFD boxes enclosing the design variable surfaces; FFD box-1 in orange; FFD box-2 in blue.

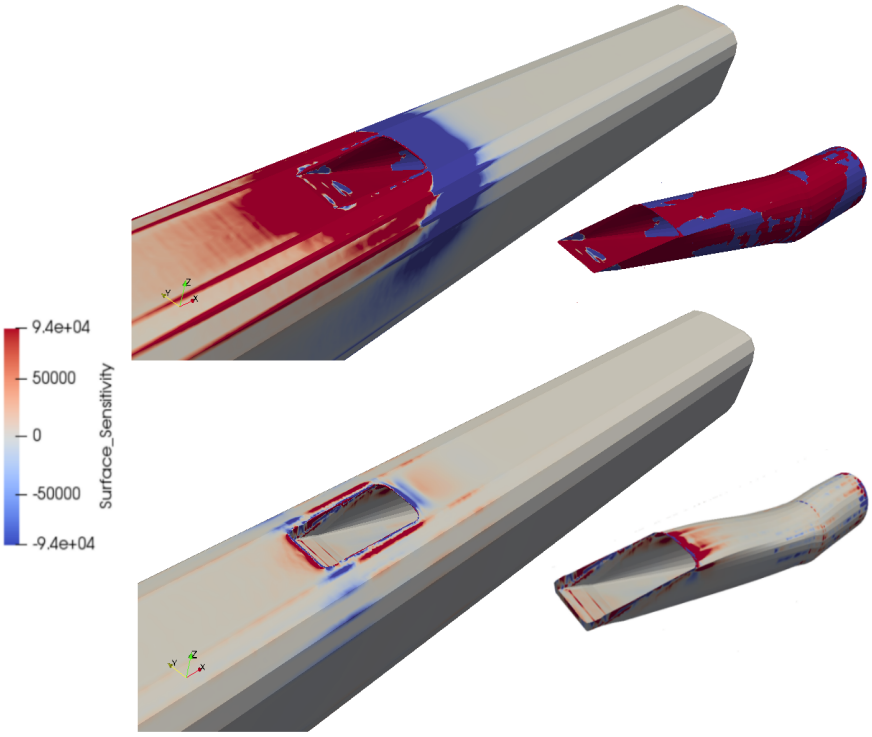

Figure 13: Surface sensitivity: Top Baseline design ; Bottom Optimum design

The design optimization stops after 25 steps when the combined objective function attains constant value. The total pressure recovery factor increases from baseline value of 0.82 to optimum value of 0.84 which is a 3 $\%$ increment considering that the full body drag constraints the optimization process. The overall lift also increases where the value of C_L/C_D of the complete vehicle increases from -0.007 to 0.011.

The shape deformation enclosed in the deformed FFD box is shown in comparison with the baseline design in figure 15.The 3D views and the center-plane cross-sectional outlines are also given in Figures 16 and 17 respectively. As illustrated, in the optimum design the upper portion of duct aft the rear lip up to the fixed duct is deformed considerably. The intake duct which is initially a straight diverging duct deforms to form a curved shaped duct. While the upper duct surface bulges towards the outer direction, lower surface bends inwards. There is a formation of a backward facing step at the onset of ramp as shown in figures. Overall the variation is prominent and duct remains flush with the body. The pressure distribution at baseline and optimum design is seen in figure 18 and 19. As observed the quality of flow improves and the pressure distribution shows an increase in the total pressure value in the optimum design as compared to the baseline. The mach filled streamlines are illustrated in figure 20. The new shape improves the flow as the re-circulation zone is reduces in size due to curvature of duct in optimum geometry compared to the straight duct of the baseline.

Hence it is observed clearly that the baseline geometry is of a fully submerged intake in which the entrance is tangential to the freestream flow while after optimization the shape remains flush.

The inlet shape is optimized for the pressure at AIP as the objective.The shape optimization of the flush inlet is performed at α =0 deg where the total pressure recovery is 82$\%$. The optimization process commences in an iterative fashion. The shape deformation process is governed by the adjoint sensitivity gradients of the design variables. Different regions of the duct are enclosed by multiple FFD boxes to ensure higher sensitivity response and deformation.

Each FFD box is of (8,8,11) configuration provides a total of 484 design variables. Once the mesh sensitivities for the combined multi-objective function are computed by the adjoint solver, they are projected onto the design variables through SU2 _DOT. The calculation of adjoint sensitivity and deformation of surface is followed in each step by flow solution for the new surface.

Table 2: Optimization summary .

	Baseline	Optimum design	Change
σ	0.82	0.845	+3 $\%$
$C_L/\ C_D$	-0.007	+0.011	+0.018
C_D	0.021	0.02045	-2.8 $\%$
DC(90)	18.1	7.7	-10.4

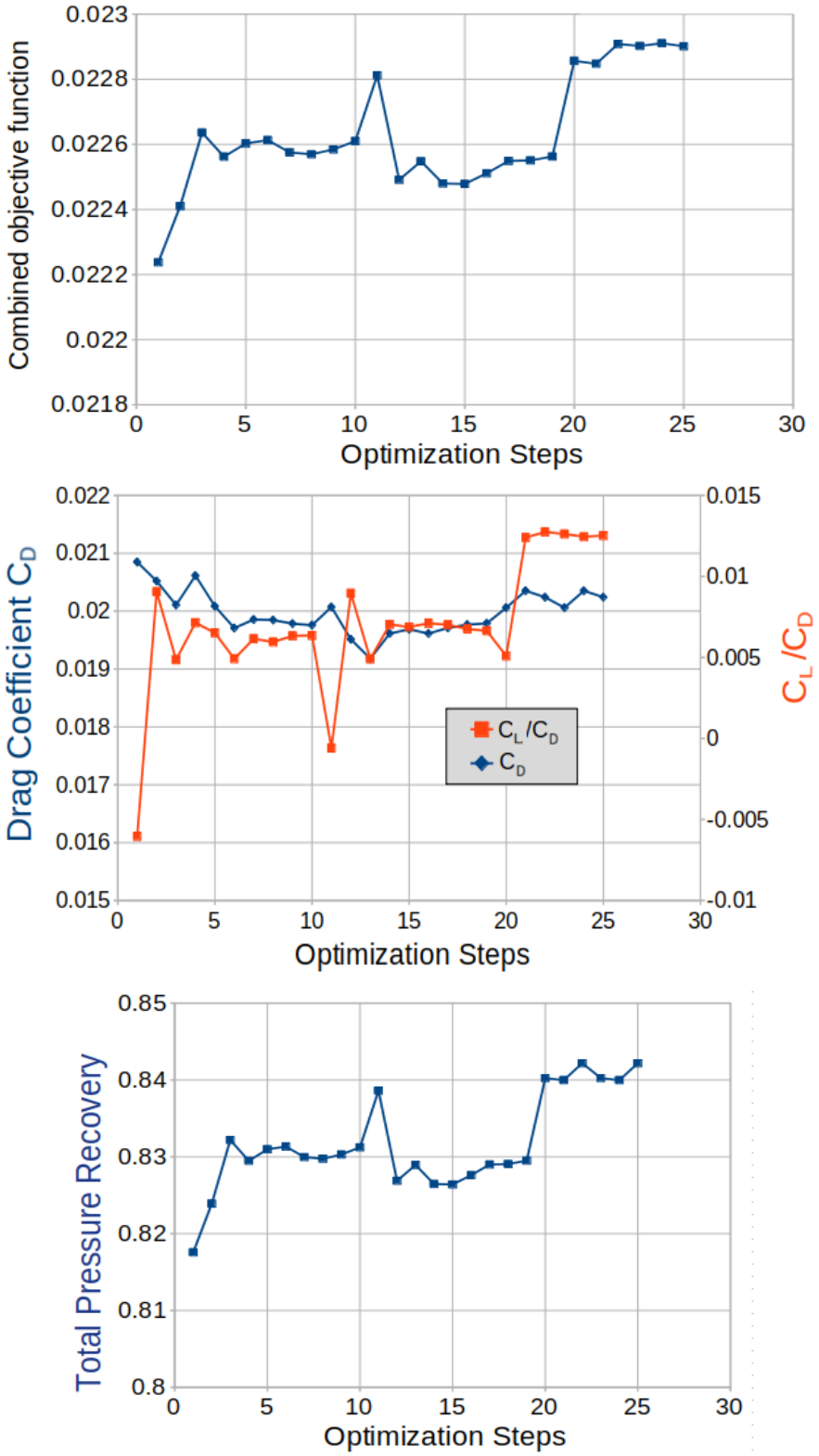

Figure 14: Optimization history C_L/C_D and σ total pressure recovery factor

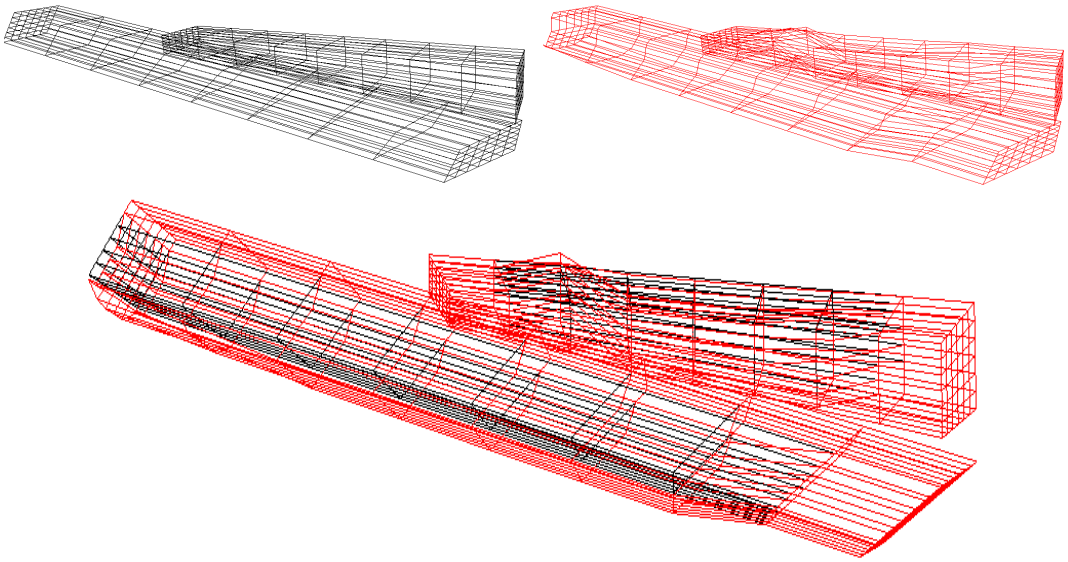

Figure 15: FFD Box deformation: Top left in Grey: Baseline ; Top right in Red: Optimum; Bottom: Overlap of baseline and deformed FFD boxes.

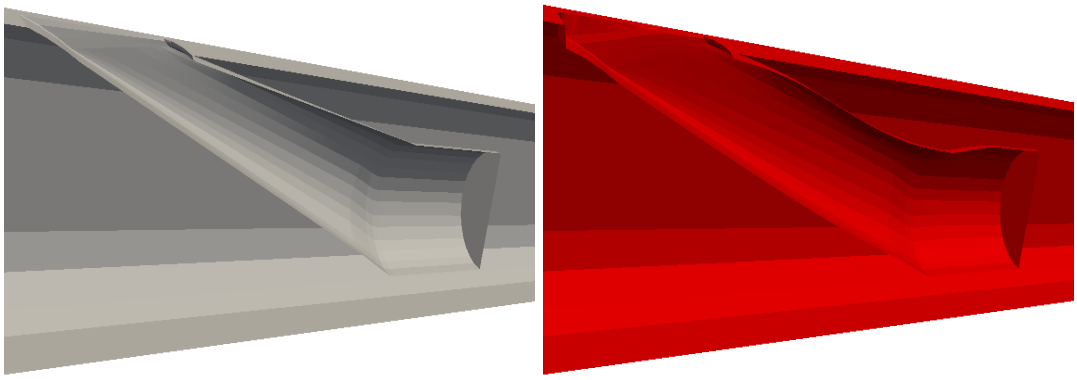

Figure 16: 3D view of shape deformation process: Left: Baseline, Right: Optimum design.

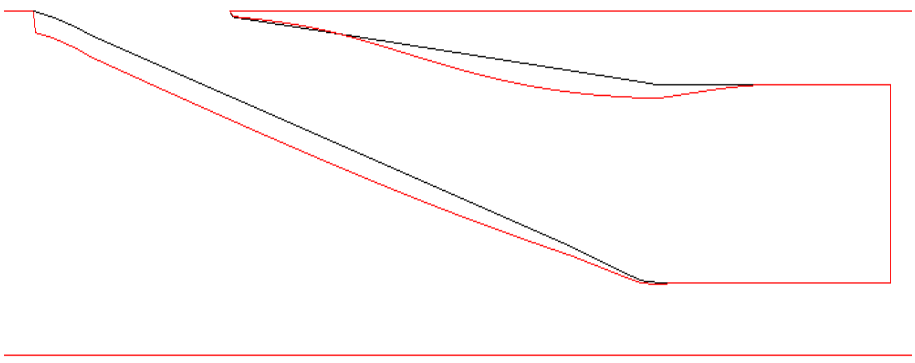

Figure 17: Intake duct at center plane : Black: Baseline, Red: optimum design.

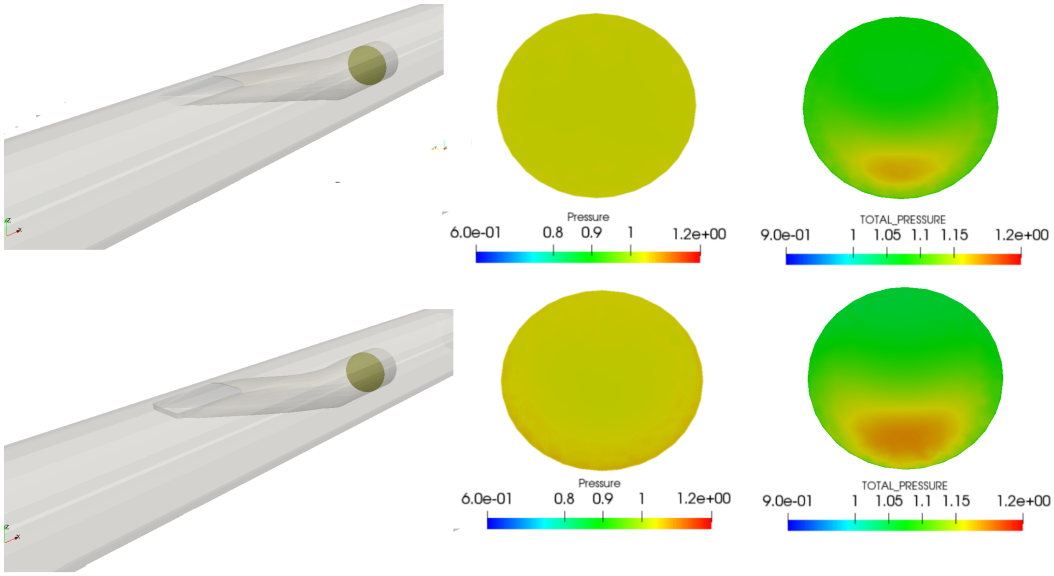

Figure 18: Pressure at AIP. Top: Baseline; Bottom: Optimum design

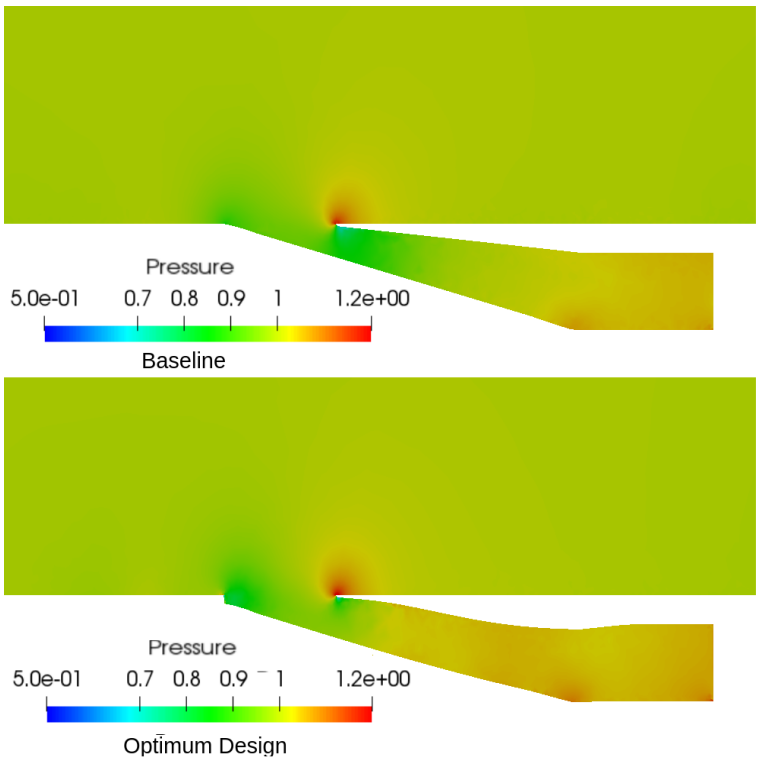

Figure 19: Pressure distribution on center-plane - Top: Baseline , Bottom: Optimum design.

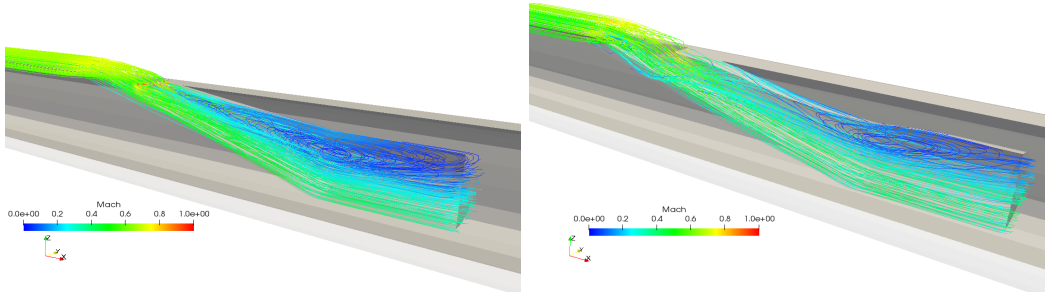

Figure 20: Stream lines coloured with Mach number. Left: Baseline; Right: Optimum design.

CONCLUSIONS

In the present study the trapezoidal flush inlet on a slender aerodynamic body was studied for multiple objectives including total pressure at AIP and lift coefficient as objectives and drag as the penalty constraint. The optimization is done using adjoint based techniques and multiple FFD boxes within SU2 platform suite. Initially the baseline configuration is verified following which the shape optimization procedure is carried out. The intake remains flush with the body during the shape deformation process. The intake internal surface is then allowed to deform along the optimization steps. The pressure recovery increases by 3% while $C_L/\ C_D$ value of 0.011 is obtained.

The study demonstrates the use of different tools for aerodynamic shape optimization specially multiple FFD boxes in different configurations can be employed for shape deformation and lift may be considered as a promising candidate as inlet design objective for future work.

References

Mossman Emmet A. and Donald E. Gault *Development of NACA Submerged Inlets and a Comparison with Wing Leading-edge Inlets for a 1/4-scale Model of a Fighter Airplane.*, NACA RM No. A7A31 August 1947.

Sun Shu, Guo Rong-Wei and Wu Yi-Zhao *Characterization and Performance Enhancement of Submerged Inlet with Flush-Mounted Planar Side Entrance*, Journal of Propulsion and Power, vol. 23, no. 5, pages: 987-995, https://doi.org/10.2514/1.26432, 2007.

Heather L. Kline *The Continuous Adjoint Mehtod for Multi-fidelity Hypersonic Inlet Design*, PhD Thesis Stanford University April 2017.

Jin Gyu Lee and Suk Jung and Chang Soo Ahn *Numerical Simulation of Three-Dimensional Flows for Flush Inlet*, 22nd Applied Aerodynamics Conference and Exhibit 2004.

Shu SUN and Rong-wei GUO *Numerical Analysis and Experimental Validation of a Submerged Inlet on the Plane Surface*, Chinese Journal of Aeronautics, vol.18 no.3, 2005.

Taskinoglu, Ezgi S. and Knight, Doyle D. *Multi-Objective Shape Optimization Study for a Subsonic Submerged Inlet*, Journal of Propulsion and Power, vol.20 no.4, 2004.

JunSok Yi and Chongam Kim and Byung Joon Lee *Multi-Objective Shape Optimization Study for a Subsonic Submerged Inlet*, Journal of Propulsion and Power, AIAA JOURNAL Vol. 50, No. 11, November 2012.

Cheng, Dai-Shu and Tan, Hui-Jun and Sun, Shu and Tong, Yue *Computational Study of a High-Performance Submerged Inlet with Bleeding Vortex*, Journal of Aircraft, AIAA JOURNAL Vol. 49, No. 3, 2012.

Sun, Shu and Tan, Hui-Jun and Wang, Chen-Xi *Submerged Inlet Performance Enhancement Using a Unique Bump-Shaped Vortex Generator*, Journal of Propulsion and Power, Journal of Propulsion and Power, AIAA JOURNAL Vol. 32, No. 5, 2016.